Structure, Vol. 8, 1189–1201, November, 2000, ©2000 Elsevier Science Ltd. All rights reserved. PII S0969-2126(00)00522-0

Crystal Structure of Protein Isoaspartyl Methyltransferase: A Catalyst for Protein Repair

Matthew M. Skinner, Joseph M. Puvathingal, Richard L. Walter,† and Alan M. Friedman*
Department of Biological Sciences
Purdue University
West Lafayette, Indiana 47907

Summary

Background: Formation of isoaspartyl residues is one of several processes that damage proteins as they age. Protein L-isoaspartate (D-aspartate) O-methyltransferase (PIMT) is a conserved and nearly ubiquitous enzyme that catalyzes the repair of proteins damaged by isoaspartyl formation.

Results: We have determined the first structure of a PIMT from crystals of the *T. maritima* enzyme complexed to S-adenosyl-L-homocysteine (AdoHcy) and refined it to 1.8 Å resolution. Although PIMT forms one structural unit, the protein can be divided functionally into three subdomains. The central subdomain closely resembles other S-adenosyl-L-methionine-dependent methyltransferases but bears a striking alteration of topological connectivity, which is not shared by any other member of this family. Rather than arranged as a mixed β sheet with topology 6↑7↓5↑4↑1↑2↑3↑, the central sheet of PIMT is reorganized to 7↑6↓5↑4↑1↑2↑3↑. AdoHcy is largely buried between the N-terminal and central subdomains by a conserved and largely hydrophobic loop on one rim of the binding cleft, and a conserved Ser/Thr-rich β strand on the other. The Ser/Thr-rich strand may provide hydrogen bonds for specific interactions with isoaspartyl substrates. The side chain of Ile-206, a conserved residue, crosses the cleft, restricting access to the donor methyl group to a deep well, the putative isoaspartyl methyl acceptor site.

Conclusions: The structure of PIMT reveals a unique modification of the methyltransferase fold along with a site for specific recognition of isoaspartyl substrates. The sequence conservation among PIMTs suggests that the current structure should prove a reliable model for understanding the repair of isoaspartyl damage in all organisms.

Introduction

Despite their general stability, proteins are often subject to chemical damage before they become substrates for physiological degradation. Thus, cells possess widespread, conserved mechanisms that can repair specific damages to proteins without requiring degradation and resynthesis. One of the best studied of these repair mechanisms is the restoration of a normal peptide backbone following the damaging isomerization that frequently occurs at asparagine and aspartate [1].

Backbone rearrangement through isoaspartyl formation (Figure 1) is linked to asparagine deamidation through a common succinimide intermediate, as demonstrated for small peptides [2, 3] and intact proteins [4–8]. The initial step in these processes is nucleophilic attack by the peptide nitrogen of the n+1 residue on the carbonyl carbon of an asparagine side chain or the carboxylate carbon of an aspartic acid side chain (Figure 1, reaction 1). In peptides this reaction occurs 10-fold more rapidly at asparagine than at aspartic acid [3, 9]. In proteins, however, there is often an aspartate that is more labile than any asparagine [5, 7, 10]. At either amino acid, nucleophilic attack by the peptide nitrogen leads to the formation of an unstable succinimide intermediate.

The succinimide intermediate is susceptible to hydrolytic attack at either carbonyl carbon. Hydrolysis at one of the carbonyl carbons restores the native backbone of the protein but results in deamidation of a former asparagine to aspartic acid (Figure 1, reaction 2). (Aspartic acid residues are unchanged in this branch of the pathway.) Hydrolysis at the other carbonyl carbon occurs approximately three times more often [7, 11–13]. It breaks the continuity of the native backbone while leaving the protein covalently connected through atoms of the former asparagine (or aspartic acid) side chain (Figure 1, reaction 3). This results in the effective addition of one methylene group to the peptide backbone and the removal of one methylene group from the side chain. These isomerized residues are called isoaspartyl (isoAsp) or β-aspartyl residues, emphasizing their β-amino acid configuration.

Other mechanisms may contribute to deamidation in intact proteins, but succinimide formation is the predominate pathway for deamidation at neutral and alkaline pH, at least for peptides [3, 9]. Succinimide formation is the only pathway which can generate those isoaspartyl residues that are frequently found at sites originally translated as asparagine or aspartate [4, 10, 13, 14]. Succinimides have also been observed directly as partially stable intermediates in several proteins, both biochemically [5–7] and in a crystal structure of hen lysozyme [8].

The susceptibility of individual asparagine and aspartate residues to this process varies considerably from protein to protein, depending on sequence context. The half-lives for asparagine in small peptides at 37°C and neutral pH range from a few hours to approximately 1 month [3, 9]. Peptides with the shortest half-life contain the sequence Asn-Gly; the next shortest half-lives occur in peptides containing asparagine followed by a medium-sized polar or nonpolar residue. Peptides with asparagine followed by larger nonpolar residues form succinimide much more slowly. Although aspartyl peptides react significantly less readily, they show a similar dependence on sequence [3, 9]. In proteins, deamidation and isoaspartyl formation also generally occur at Asn/Asp-Gly/Ser sequences.

Conformational flexibility is required for this pathway [15, 16], although it is far from completely inhibited in native proteins. Even within a well-ordered and disulfide-restrained loop, Asn-67 of RNase A has a half-life of only 7.4 days at 37°C and pH 8.2 [13]. Although generally reacting more slowly than this, many proteins exhibit multiple sites of isoaspartyl formation after in vitro incubation at 37°C and pH 7.4 [6, 10]. Many of these sites were discovered during the unusually careful scrutiny that

*To whom correspondence should be addressed (e-mail: afried@bilbo.bio.purdue.edu).
†Present address: Procter & Gamble, Cincinnati, Ohio.

Key words: protein deamidation; isoaspartate; protein repair; aging; methyltransferase

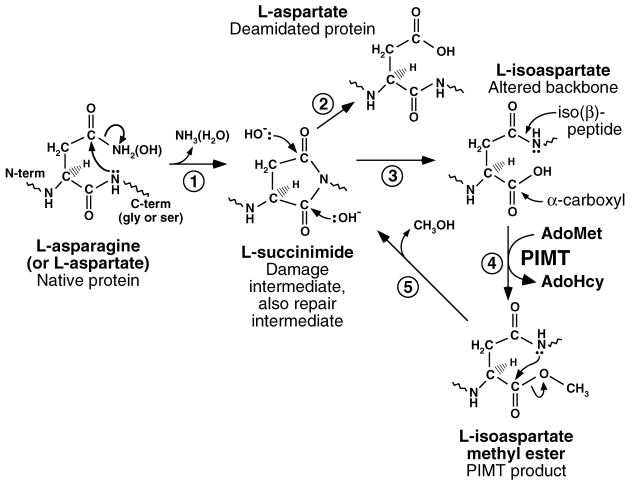

Figure 1. Protein Deamidation, Isoaspartyl Formation, and the Repair Cycle Catalyzed by PIMT

The succinimide-based mechanism for deamidation and isoaspartyl formation was originally developed in studies on model amides [2]. The protein repair cycle of PIMT is as proposed [11, 12].

accompanies the development of protein pharmaceuticals, suggesting that many more examples could be found. Isoaspartyl residues have been observed by NMR in calbindin [16] and in crystal structures of RNase A [17], RNase U2 [18], and hen lysozyme [8]. As in RNase A, these isoaspartyl residues are located in surface loops.

The formation of isoaspartyl residues often results in a significant loss of protein function [13, 16, 19, 20]. The potential physiological damage caused by the isoaspartyl branch of this pathway can be seen in the nearly universal occurrence of a repair process. The enzyme protein L-isoaspartate (D-aspartate) O-methyltransferase (EC 2.1.1.77) initiates repair of the isoaspartyl product. PIMT activity has been detected in all plants [21], animals [21, 22], and bacteria [22, 23] tested. Homologs have been identified in nearly all sequenced genomes.

PIMT catalyzes the transfer of a methyl group from S-adenosyl-L-methionine (AdoMet) to the α-carboxylate side chain of the isoaspartyl residue (Figure 1, reaction 4). Through this transfer, the isoaspartyl group becomes activated for conversion back to the succinimide by a nonenzymatic reaction (Figure 1, reaction 5). Once back in the succinimide form, hydrolysis can again occur at either carbonyl carbon, converting the protein to the aspartate form or regenerating the isoaspartate.

This process cannot restore the amino group to the side chain of an original asparagine, but the pathway can restore the correct configuration to the protein backbone. The resulting deamidated asparagine (that is, aspartate) residue is known to be generally less damaging to protein structure and function than is the isoaspartyl configuration [7, 16, 19, 20]. With continued methyl group input from the physiological pool of AdoMet, the repair reaction cycle can continue indefinitely. Each round converts a fraction of the isoaspartyl residues to the less damaged aspartyl form. This repair process has been reconstituted in vitro with isoaspartyl-modified calmodulin, purified PIMT, and an excess of AdoMet, resulting in the conversion of approximately half of isoaspartyl calmodulin to the aspartyl form and restoration of 30%–50% of native activity [19]. While it

Table 1. Structure Determination Statistics

	Native (Cd)[a]	Native (Zn)[b]	Trimethyl-Lead Acetate I[c]	Trimethyl-Lead Acetate II[d]	$KAuCl_4$[e]	$UO_2(OAc)_2$[f]	$Sm(OAc)_3$[g]
Data Collection Statistics							
Diffraction limit (Å)	1.65	1.7	1.65	1.65	2.5	2.5	1.9
Completeness (%)	97.6	99.1	98.4	98.1	96.8	96.4	87.6
R_{merge}[h] (%)	5.3	5.2	5.6	4.6	8.7	7.8	7.9
R_{iso}[i] (%)	N.A.	20.0	11.3	21.1	23.7	14.6	17.0
Phase Determination Statistics							
Resolution limit for phasing	1.65	2.0	2.2	2.2	2.5	2.5	2.5
Phasing Power[j]							
$Isomorphous_{centric}$	N.A.	0.06	0.67	0.89	0.81	0.49	0.56
$Isomorphous_{acentric}$	N.A.	0.05	0.55	0.64	0.63	0.36	0.44
Anomalous	0.44	0.02	0.88	0.77	0.28	0.12	0.49
Figure of merit[k]							
Centric	0.42						
Acentric	0.38						
Overall	0.38						
After density mod.	0.58						

[a] Native crystal grown with 100 mM $CdCl_2$ (Fluka).
[b] Native crystal grown with 100 mM $ZnSO_4$ (Fluka).
[c] Cd-native crystal soaked in 40 mM Trimethyllead acetate (Alfa) for 14 days.
[d] Cd-native crystal soaked in 120 mM Trimethyllead acetate (Alfa) for 14 days.
[e] Cd-native crystal soaked in 0.1 mM $KAuCl_4$ (Aesar) for 18 hr.
[f] Cd-native crystal soaked in 0.5 mM $UO_2(OAc)_2$ (Fisher) for 42 hr.
[g] Cd-native crystal soaked in 10 mM $Sm(OAc)_3$ (Alfa) for 19 hr.
[h] $R_{merge} = \Sigma\ |I_{obs} - <I>|/\Sigma I_{obs}$
[i] $R_{iso} = \Sigma\ |F_{PH} - F_P|/\Sigma|F_P|$, where F_P and F_{PH} are the structure factor amplitudes of the native and derivative.
[j] Isomorphous phasing power is defined as $<|\Delta F_H|>/rms(\epsilon)$, where $<|\Delta F_H|>$ is the mean calculated amplitude for the heavy atom model and rms(ϵ) is the root mean square lack of closure error for the isomorphous differences. Anomalous phasing power is defined as $<|\Delta F_{calc}|>/rms(\epsilon)$, where $<|\Delta F_{calc}|>$ is the mean calculated Bijvoet difference for the heavy atom model and rms(ϵ) is the root mean square lack of closure error for the anomalous differences.
[k] Figure of merit is defined as $m = \int P(\alpha)\exp(i\alpha)d\alpha / \int P(\alpha)d\alpha$.

Table 2. Refinement Statistics	
Refinement Statistics	
Resolution range (Å)	15–1.8 Å
Number of reflections ($\|F\|>2\ \sigma$)	66,308
R factor[a]	
Working (%)	18.2
Free (%)	20.3
Model Statistics	
Protein atoms	5,106
AdoHcy atoms	52
Cd and Cl atoms	19
Water molecules	463
Rmsd[b] bonds (Å)	0.006
angles (°)	1.38

[a] Crystallographic residual is defined as $R = \Sigma|F_{obs} - F_{calc}|/\Sigma|F_{obs}|$, where F_{obs} and F_{calc} are the observed and calculated structure factor amplitudes. The summations for the free R factor are taken over a random 5% of the reflection data that were omitted from the target function for all stages of refinement.
[b] Root mean square deviation (rmsd) from ideal stereochemistry.

cannot restore asparagine, this process *can* return proteins bearing isoaspartyl groups generated from aspartate residues [5, 7] to their original form.

The repair activity catalyzed by PIMT is essential for prolonged life in higher organisms. Mice lacking functional PIMT accumulate isoaspartyl proteins and do not survive beyond an average lifespan of 6 weeks, dying suddenly from seizures [24]. In *E. coli*, mutations in PIMT decrease survival of stationary phase cells subjected to an additional environmental stress [25]. The widespread occurrence and strong sequence conservation of PIMT among many organisms suggests both the importance of PIMT and preservation of its role and mechanism across archaea, eubacteria, and eukaryota.

The rate of protein damage due to isoaspartyl formation should be greatly elevated in the hyperthermophile *Thermotoga maritima* at its 80°C growth temperature. *T. maritima* might be expected to have an especially effective PIMT. At its activity optimum of 85°C, *T. maritima* PIMT has a V_{max} 10-fold faster than that of PIMTs from mesophilic organisms assayed at 25°C–37°C with a K_m for isoAsp peptides similar to that of many other species [26]. These kinetic constants suggest that the *Thermotoga* enzyme is a very effective form of PIMT, adapted to extreme conditions. We have determined the crystal structure of *T. maritima* PIMT as an initial step in understanding the structural basis of this important biological repair system.

Results and Discussion

Structure Determination

The structure was determined by multiple isomorphous replacement and anomalous scattering using native crystals grown in $CdCl_2$ or $ZnSO_4$ and derivative crystals created by soaking in heavy atom solutions (Table 1). The experimental phases were improved by density modification and multiple automated refinement to yield an excellent electron density map entirely without ambiguous regions. Model building and refinement yielded a final R factor of 18.2% (R_{free} = 20.3%) with excellent stereochemistry (Table 2). All nonglycine, nonproline residues are in either the "most favored" (89.9%) or "additional allowed" (10.1%) regions of the Ramachandran plot [27].

Overall Architecture: Three Subdomains

T. maritima PIMT forms a mixed α/β protein shaped like a cylinder approximately 65 Å long and 30 Å in diameter (Figure 2). There is continuity in hydrogen bonding and packing of a hydrophobic core throughout the molecule, but *T. maritima* PIMT can also be divided into three functional subdomains (Figure 2a, indicated in red, green, and blue), representing distinct volumes in the structure. The central subdomain contains a modified methyltransferase fold [28] common to many AdoMet-dependent methyltransferases (AdoMet-MTases). In labeling the secondary structure elements of PIMT (Figures 2b and 3a), we have followed earlier descriptions of the AdoMet-MTase fold [28, 29], employing numbers to indicate strands and capital letters to indicate helices within the fold. Outside the canonical fold, helices are numbered and strands are denoted by lower case letters.

The N terminus begins a largely helical subdomain (Figure 2a, red, residues 1–77) that packs against the N-terminal half

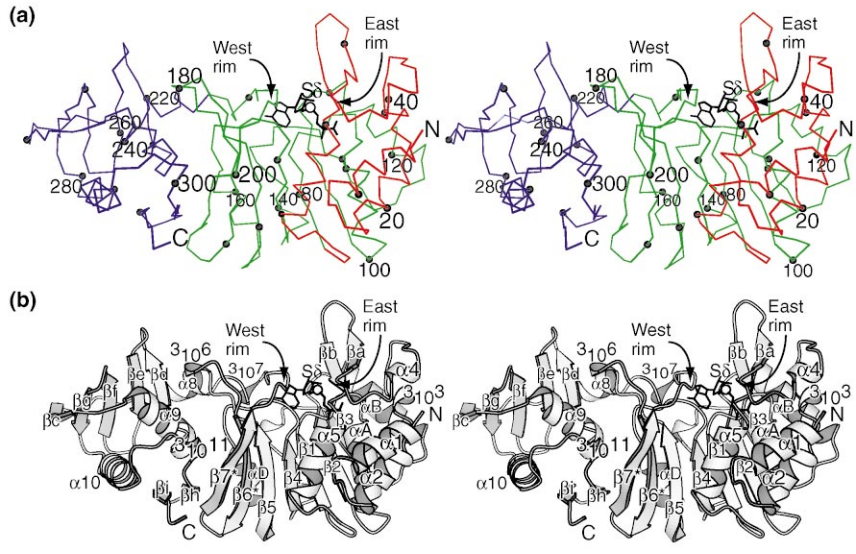

Figure 2. Cα Backbone and Secondary Structure Elements of *T. maritima* PIMT

(a) Stereo diagram of the Cα backbone. The N and C termini and every tenth residue are marked. AdoHcy is shown as a stick model with the Sδ atom, the site of methyl group transfer, drawn as a white sphere. The approximate locations of the East and West Rims are indicated.

(b) Stereo diagram of secondary structure elements. For clarity not all secondary structure elements are labeled. AdoHcy is drawn as in (a). This figure was prepared using MOLSCRIPT [59].

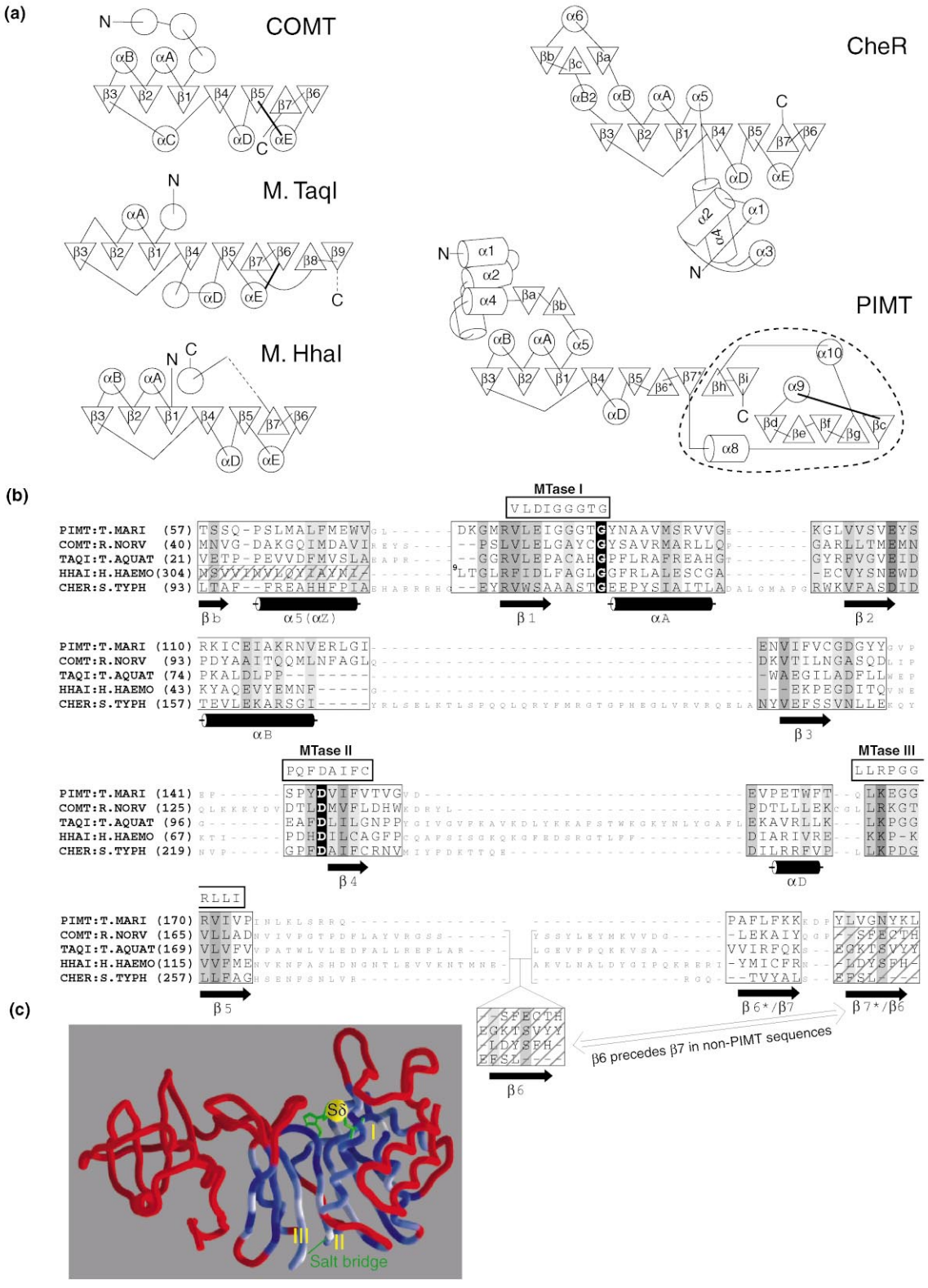

Figure 3. Structure and Sequence Conservation in the AdoMet-MTase Family

(a) Topology diagrams of representative AdoMet-MTases: catechol-O-methyltransferase (COMT, 1vid) [30], the TaqI (2ADM)[60] and HhaI (10MH)[36] DNA methyltransferases, the chemotaxis receptor methyltransferase from *S. typhimurium* (CheR, 1AF7) [29], and *T. maritima* PIMT. Helices and strands that run perpendicular to the plane of the figure are drawn as circles and triangles, respectively, while helices and strands running parallel to the figure are depicted as arrows and cylinders. Triangles pointing down indicate a strand whose C terminus is towards the viewer. Strands and helices are labeled according to

of the central subdomain. Between α4 and α5 this subdomain projects a β hairpin of strands βa and βb, which extends above the AdoHcy binding site. Strand βb and Val-45 of βa form a ridge along one side of the AdoHcy binding cleft. We call this ridge the "East Rim" and propose that it plays an important role in substrate recognition. The N-terminal subdomain appears to be the PIMT analog of the largely helical substrate recognition domains found at the N termini of the chemotaxis receptor methylase CheR [29] and catechol O-methyltransferase (COMT) [30]. There is no global structural or sequence similarity to the N-terminal domains of CheR or COMT, however. Searching the DALI database [31] with this subdomain yields only a small number of weak matches ($Z \leq 2.6\ \sigma$), none of which appear to be functionally related.

The central subdomain (Figure 2a, green, residues 78–214) contains an AdoMet-MTase fold, a modified Rossmann-type nucleotide binding fold, with a mixed seven-stranded β sheet flanked by α helices on both sides (Figure 2b). While there are important differences between PIMT and the other AdoMet-MTases in the architecture of this domain (see below), the PIMT fold is still very similar to the one conserved within the diverse family of AdoMet-MTases (Figure 3a) [28].

In the AdoMet-MTase fold, the first five strands are parallel while the C-terminal part of the sheet contains two antiparallel β strands. In all other AdoMet-MTases of known structure, the last parallel strand, β5, connects to helix αE, which then skips over one strand in the sheet to connect to the outside strand, β6. β6 then connects to β7 through a β hairpin, forming a 6↑7↓5↑4↑1↑2↑3↑ topology.

In PIMT, the last third of the AdoMet-MTase fold is significantly altered. Helix αE is missing. Instead of skipping over a strand, β5 connects directly to the adjacent strand in the sheet through an extended loop. The result is a topological reordering of strands β6 and β7 of the AdoMet-MTase fold so that we now call them β6* and β7* in PIMT (Figure 3a). In PIMT β5 connects directly to the adjacent β6*, which connects to the adjacent β7* through a β hairpin. Thus β7* in PIMT is located where β6 is in the other AdoMet-MTases, and the sheet is 7*↑6*↓5↑4↑1↑2↑3↑. Remarkably, PIMT preserves the parallel/antiparallel organization of the other AdoMet-MTases while connecting the strands in a different order. Although unprecedented relative to other AdoMet-MTases, we expect that this topology will be maintained in all PIMTs due to a high level of sequence conservation in this region (Figure 4).

The topological rearrangement of the β sheet is accompanied by the formation of a functionally important substructure following strand β7*. Residues following β7 at the end of the subdomain form a ridge, the "West Rim," opposite βb of the N-terminal subdomain, the East Rim (Figures 2 and 5). Between the two rims lies a cleft that contains AdoHcy in the present structure and is the presumed active site.

The C-terminal subdomain (Figure 2a, blue, residues 215–317) is unique to the PIMT from *T. maritima*. Similar sequences have not been found in PIMTs from other species or in any other AdoMet-MTase. These sequences form an α+β subdomain, including a five-stranded β meander flanked on both sides by α helices. Although the C-terminal subdomain is dominated by the common β meander motif, it has only weak similarities to other proteins in the DALI database [31]. The role of the C-terminal subdomain is unclear. C-terminal deletions lead to a loss of PIMT activity [26], but this could be a folding and/or stability defect.

Comparison with PIMT from Other Organisms

PIMTs from various organisms form a family of rather highly conserved sequences. PIMT from the deeply rooted eubacterium *T. maritima* still exhibits 31% sequence identity with the *E. coli* enzyme and 26% identity to human [26]. The structure of *T. maritima* PIMT allows us to accurately realign PIMT sequences from various species (Figure 4). This alignment was developed by manually readjusting a ClustalW [32] alignment so that gaps fall in loop regions and residues with identifiably important functions are maximally conserved.

Not surprisingly, the three sequence motifs previously noted as being shared among AdoMet-MTases [33] are considerably less variable in the PIMT sequences. We call these less variable sequences MTase-in-PIMT motifs ("MTase/PIMT" in Figure 4). The addition of structural information also allows us to add to and improve upon the PIMT-specific premotif I (our PIMT III, which forms the East Rim) and postmotif III (our PIMT XII, which forms the West Rim), which were previously identified in an alignment of prokaryotic PIMTs [26].

Comparison with Other AdoMet-MTases: Conservation of the AdoMet-MTase Fold

We aligned 12 members of the AdoMet-MTase family of known structure onto PIMT by two independent methods (Table 3). Although the recent structures of the protein arginine methyltransferase 3 [34] and the RNA methyltransferase FtsJ [35] are not included in the alignment, both of them also bear an AdoMet-MTase fold. As expected in a widely diverged family of proteins, both the number of Cα atoms that aligned with PIMT and their root mean square deviation (rmsd) varies greatly among the proteins. There is no clear pattern that suggests PIMT is most closely related to any group of AdoMet-MTases. The two methods do give somewhat comparable rankings of the similarity of individual AdoMet-MTases to PIMT, though, with COMT, fibrillarin, glycine N-methyltransferase, ErmC, and CheR as the most similar. In general, the DNA methyltransferases are less similar to PIMT.

We compiled a structure-based sequence alignment of the

the uniform nomenclature for AdoMet-MTases [28, 29]. The helix we call α5 has also been called αZ. The dashed lines in M. HhaI and M. TaqI indicate the additional target recognition domain. The elements encircled by the dashed line in PIMT represent the C-terminal subdomain that is unique to *T. maritima*.
(b) A portion of the structure-based sequence alignment of the AdoMet-MTases. Structures were superimposed as described in Experimental Procedures (Table 3) using the lsq_explicit and lsq_improve options in the program O [49]. Only the core methyltransferase fold and the often conserved βb/α5 extension are shown. The secondary structural elements of *T. maritima* PIMT are shown below the amino acid sequence. Boxed residues represent regions of structural alignment, while the smaller type indicates those sequences outside of the aligned regions. Invariant residues are in inverse type, while highly conserved to less conserved residues as determined by MaxHom [61] are shaded from dark gray to lighter gray. Three sequence motifs conserved among the AdoMet-MTases [33] are indicated along with the most frequent residue at each position. The crosshatched regions represent differences in sequence order relative to *T. maritima* PIMT. This panel was prepared with the program ALSCRIPT [62].
(c) Sequence conservation of the methyltransferase family plotted on the structure of *T. maritima* PIMT. Sequence conservation as in (b) was shaded from white (high conservation) to dark blue (low conservation). Regions that have no structural alignment are shown in red. The approximate locations of the three conserved MTase motifs are indicated. This panel was prepared with GRASP [52].

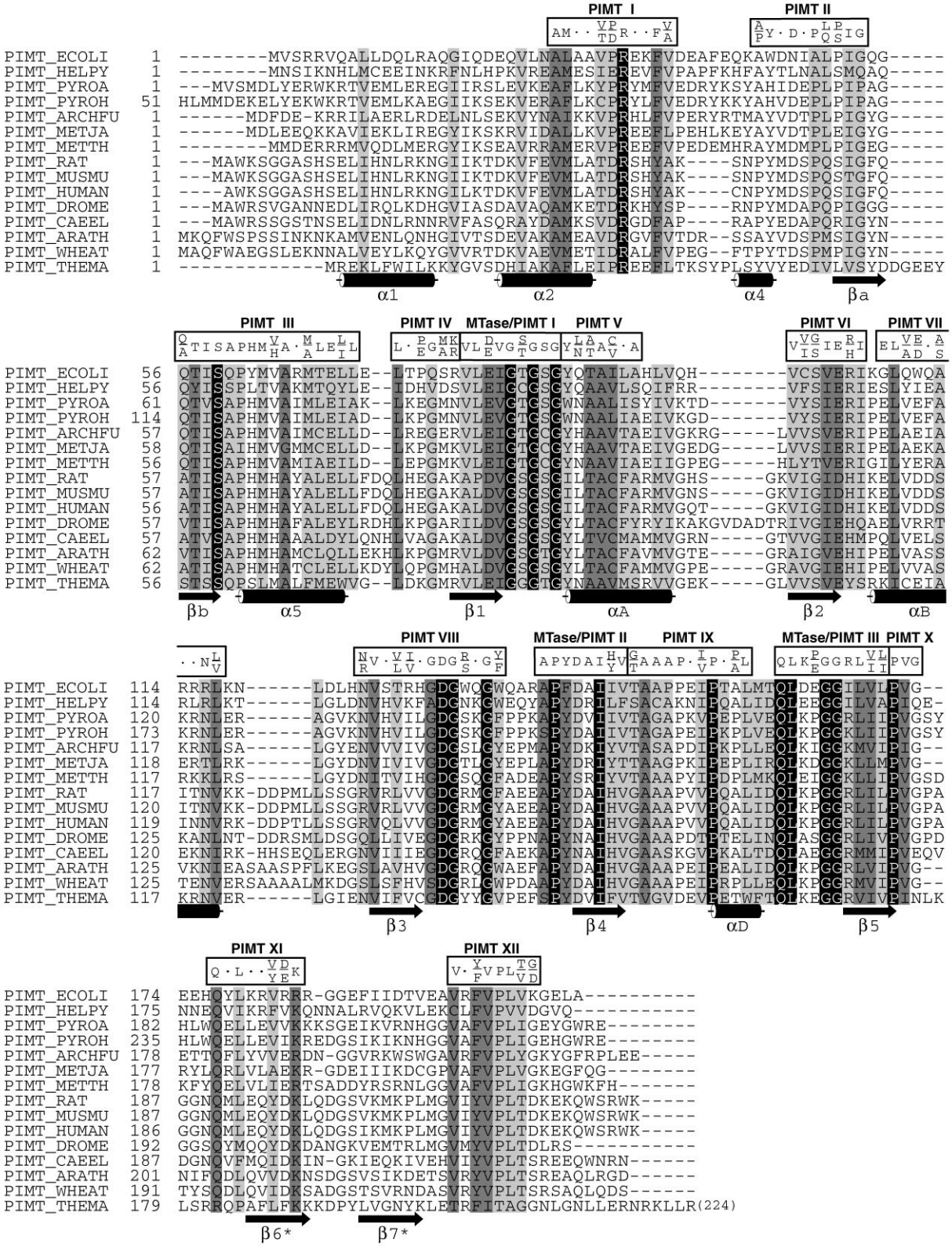

Figure 4. Structure-Based Alignment of PIMT Sequences from Various Organisms

Aligned sequences (see text) representing organisms from eubacteria (top), archaea (middle), and eukaryota (bottom) are shown. PIMT homologs are those of *Escherichia coli* and *Helicobacter pylori* from the eubacteria; *Pyrococcus abyssi*, *Pyrococcus horikoshii*, *Archaeoglobus fulgidus*, *Methanococcus jannaschii*, and *Methanobacterium thermoautotrophicum* from the archaea; rat, mouse, human, *Drosophila melanogaster*, *Caenorhabditis elegans*, *Arabidopsis thaliana*,

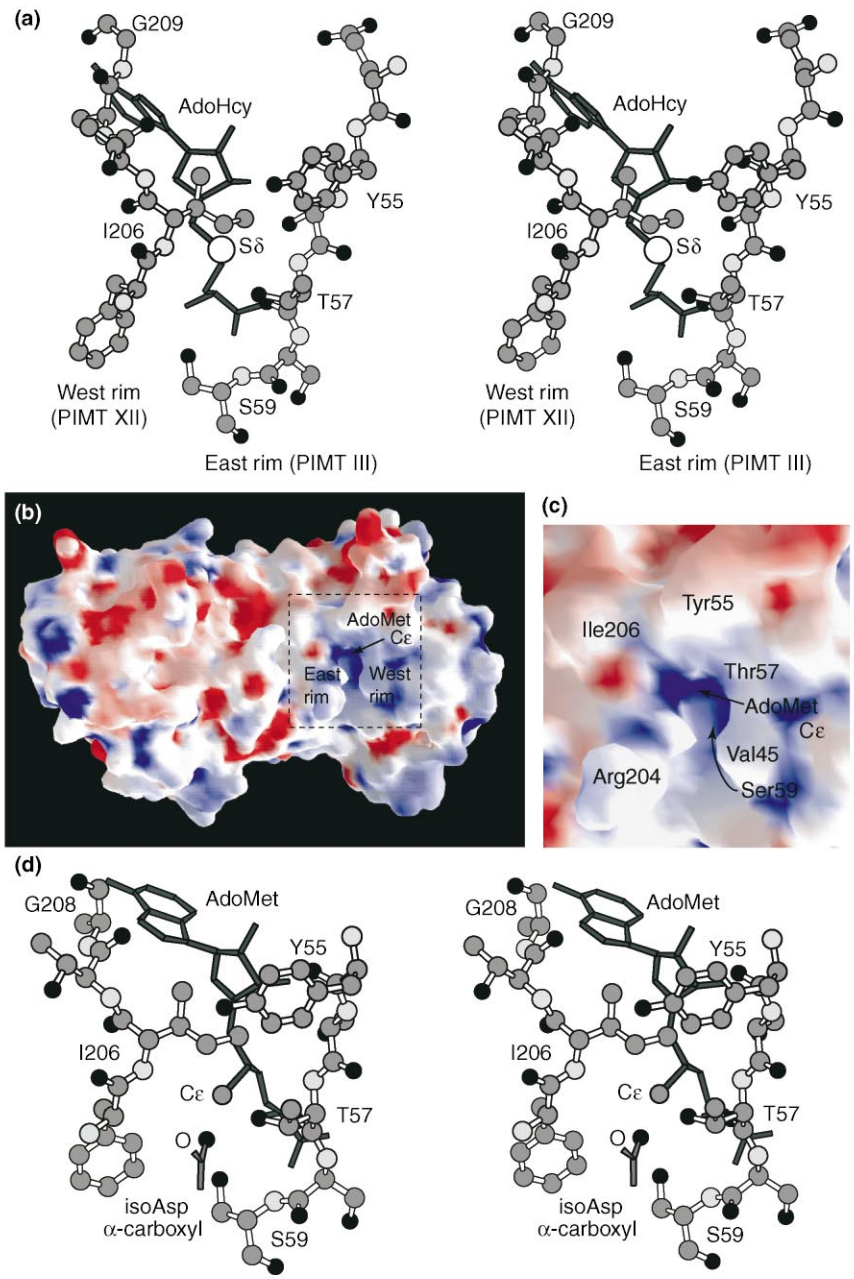

Figure 5. Active Site Structure and a Model for Isoaspartyl Peptide Binding

(a) Stereo diagram of AdoHcy and surrounding surface residues. Only AdoHcy and the residues on either side are shown. Other residues, including the overlying Val-45, have been removed for clarity. The protein is shown as a ball and stick model, while the bonds of AdoHcy are drawn as gray sticks. The Sδ atom of AdoHcy is depicted as a white sphere.

(b) Electrostatic surface potential of *T. maritima* PIMT with modeled AdoMet. Electrostatic surface potential was calculated and displayed with the program GRASP [52]. Fully saturated blue and red correspond to potentials of $+10$ k_BT/q and -10 k_BT/q. The locations of the East and West Rims and the Cϵ atom of AdoMet are indicated. The view shown is approximately the same as Figure 2.

(c) Closeup of (b) centered around the active site, the dashed box in (b). The surface location of residues near the the active site are noted.

(d) Stereo diagram of the proposed model for isoaspartyl peptide binding (see text). The α-carboxyl group of the isoAsp is shown entering the deep well containing the modeled methyl group donor. The location of the remaining atoms of the isoaspartyl residue and the rest of a bound isoAsp peptide can not be predicted with confidence. Panels (a) and (d) were drawn with the program MOLSCRIPT [59].

AdoMet-dependent methyltransferases (Figure 3b). The inverted relationship between β6 and β7 of most AdoMet-MTases and β6* and β7* of PIMT is evident as is the sequence permutation of M. HhaI relative to PIMT and the other listed AdoMet-MTases (Figure 3b, doubled arrow-headed line and crosshatched boxes). The previously described AdoMet-MTase sequence motifs [33] cover most of the regions of greatest conservation in our alignment, but additional regions of relative conservation are also evident, especially in strand β2.

The extent of sequence conservation in the structurally aligned regions of the AdoMet-MTases has been plotted onto the structure of PIMT (Figure 3c). While several of the most highly conserved residues (in white) are located in the AdoHcy/AdoMet binding site, the greatest sequence conservation oc-

and wheat from the eukaryota; and the PIMT from *T. maritima* at the bottom, immediately above its secondary structure elements. Invariant residues are displayed in inverse type, while highly conserved to less conserved residues are shaded from dark gray to lighter gray. Conserved sequence motifs are boxed above the sequences. Where only one or two residues are found in 10 or more out of the 15 aligned sequences, those residue(s) are noted. The PIMT version of previously identified AdoMet-MTase consensus sequences [33] form the MTase-in-PIMT motifs, indicated by "MTase/PIMT". Conserved sequences unique to PIMT are indicated by "PIMT." This figure was prepared with the program ALSCRIPT [62].

curs in the core regions of β strands 1, 2, 4, and 5. The higher level of conservation in the β strands suggests a crucial role for these residues in maintaining the AdoMet-MTase fold. The structural and sequence conservation of the β sheet is supplemented by the frequent maintenance of a salt bridge (Figure 3c) between an Asp immediately before β4 (Asp-146 in PIMT) and a Lys or Arg in the loop between αD and β5 (Lys-166 in PIMT). A salt bridge at precisely equivalent residues is present in 8 of 13 AdoMet-MTases. An additional 4 of 13 have an alternate salt bridge between these two structural elements, employing nearby residues. Future analysis will be needed to determine any potential role for the salt bridge in stabilizing the fold and also to explain why greater sequence conservation appears to be required to maintain the β sheet than to maintain the AdoHcy/AdoMet binding site.

The Active Site: AdoHcy/AdoMet Recognition

DNA (cytosine-5)-methyltransferases employ cysteine to generate a covalent enzyme-substrate intermediate with enhanced nucleophilicity [36, 37]. In most AdoMet-Mtases, however, unmodified substrate nucleophiles attack the AdoMet Cε directly, either with [30] or without [29, 38, 39] the aid of a metal ion. PIMT was thought to function without a covalent intermediate and without the aid of metal ions. This is confirmed; there are no cysteines near the active site, nor are there bound ions or any obvious metal ligands. Apparently, the O of the isoaspartyl α-carboxylate is a strong enough nucleophile that neither a covalent intermediate nor a metal ion is required.

The AdoHcy/AdoMet binding site in PIMT follows the general AdoMet-MTase pattern in exhibiting strong structural similarity and weak sequence conservation with other AdoMet-MTases [29]. However, many of the residues that make specific hydrogen bonding or close nonbonded contact with AdoHcy are invariant or highly conserved within the PIMTs from various organisms. These residues include Gly-83, Gly-85, and Gly-87 and Glu-107, which interact with the ribose and methionine moieties, and Val-106, Asp-134, and Gly-135, which interact with the base. The conformation of the loop between β1 and αA, a key element in positioning AdoMet, is very similar to nearly all other AdoMet-MTases (Table 3, initial explicit alignment).

The Active Site: Isoaspartyl Peptide Recognition

The sequence conservation of PIMT motif III, forming the East Rim, and of PIMT motif XII, forming the West Rim, suggests important and constant roles for these substructures. Strand βb of the East Rim includes residues 55–59, with the sequence Tyr-Ser-Thr-Ser-Ser in *T. maritima* and significant hydrogen bonding potential in all PIMT's (Figure 4). As judged by the AdoHcy binding site in PIMT (Figures 2 and 5), these residues are located in a position to interact with isoaspartyl substrates. We propose that the isoaspartyl peptide is recognized specifically through the hydrogen bonding potential of these residues.

The side chains of Thr-57 and Ser-59 (and perhaps Tyr-55) may be key elements in recognizing the isoaspartyl substrate and distinguishing it from the large background of normal aspartyl residues and other carboxylates in the cell. Ser-59 is invariant in PIMT, and Thr-57, almost so. The conservation of Tyr-55 (and of its hydrogen bonding potential) is difficult to judge since the residue is near a sequence insertion which lengthens the βa/βb hairpin in *T. maritima*. All other species (except *D. melanogaster*) contain Asn or Gln near the position of Tyr-55. These residues may provide equivalent hydrogen bonding potential.

These putative specificity-determining residues of βb are located in a position similar to the linker between N- and C-terminal domains of CheR and COMT. This linker region is thought to control substrate specificity in CheR [29], while linker residues Trp-38 and Met-40 form one face of the catechol binding site in the COMT:3,5-dinitrocatechol complex [30]. In 10 out of the 13 aligned AdoMet-Mtases, there is a short stretch of extended conformation in a position similar to that of strand βb. These extended conformation residues preceding α5 do not form full β strands as determined by the common algorithm of Kabsch and Sander [40] except in PIMT. That algorithm requires β strands to be hydrogen bonded to another β strand, a situation that occurs only in the βa/βb hairpin of PIMT.

A striking feature of the active site is that solvent access to AdoHcy is blocked over much of the molecule, most notably by Ile-206, whose side chain lies directly over the Sδ atom (Figure 5). This residue is nearly invariant, a valine in all other PIMTs (Figure 4). When examined as a molecular surface (Figures 5b–5c), Ile-206 merges with Thr-57 and Tyr-55 to form a solid "bridge" over the AdoMet binding site.

While this bridge largely blocks access to Sδ, a Cε methyl group that we have modeled onto the AdoHcy (see below) to mimic bound AdoMet would be accessible to nucleophilic attack, although access is limited to one direction. The donor methyl group of the modeled AdoMet would be accessible only through a deep well in the protein surface (Figures 5b–5c). While there is also the possibility of a significant difference in the conformation of Ile-206 in PIMT complexed with AdoMet (see below), restricted access to the AdoMet Cε may be an important feature in controlling the reactivity of the cofactor.

To be effective as a general protein repair catalyst, PIMT must be able to recognize substrates not limited to specific sites of isoAsp formation on specific proteins. Instead, PIMT should recognize isoAsp residues in the widest possible variety of contexts. Confirming its potential utility as a repair enzyme, PIMT has been found to react substoichiometrically with nearly all erythrocyte proteins in vivo [41]. These sites presumably represent the substoichiometric accumulation of isoaspartate in nearly all proteins.

Despite PIMT's functional versatility, the *T. maritima* enzyme forms a single, apparently rigid stucture for binding isoAsp peptides in the curent crystal. Based on the K_m of various peptide substrates for the human enzyme, PIMT forms a binding site for 4–6 residues [42]. The surface of PIMT around the active site contains specific hydrogen bonding and electrostatic potentials as well as neutral and hydrophobic patches (Figure 5B). The properties of this surface in the human enzyme must presumably explain the observed preferences of that PIMT (and maybe all PIMTs) for bulky residues preceding the isoAsp and for neutral and positive residues following it [42].

Future studies may yield more insight into potential plasticity of the peptide binding site. At present, though, it appears that largely fixed surfaces in PIMT provide the basis on which all substrates interact with the enzyme. Given the ordered state of the PIMT active site and surrounding surfaces, it is surprising that intact protein substrates have a similar range of affinity for the enzyme, as do free peptides [42, 43]. This is not absolute, though, and a large reduction in the ability of PIMT to methylate several intact proteins relative to isoaspartyl peptides derived from them [42, 43] suggests a role for conformation of enzyme and substrate. The apparent contradiction may simply be a measure of the evolved effectiveness of PIMT in methylating

Table 3. Methyltransferase Structure Alignments

			Least Squares Superposition in O[a]					DALI Superposition[b]			
			Initial Explicit[c]		Final Improved[d]						
Name	PDB Entry	Reference	Rmsd	Identity (%)[e]	Rmsd	Number of Cα	Identity (%)[f]	Z Score	Rmsd	Number of Cα	Identity (%)[g]
DNA methyltransferases											
M. HhaI	10MH	[36]	0.97	13	1.58	52	19	3.4	3.5	106	12
M HaeIII	1DCT	[37]	0.74	13	2.18	102	12	4.0	12.1	115	12
DpnM (M. DpnII)	2DPM	[53]	1.25	19	2.10	89	11	5.6	3.3	130	10
M. PvuII	1BOO	[54]	1.42	31	2.11	113	18	2.7	3.6	116	10
M. TaqI	2ADM	[38]	1.32	25	1.77	57	21	6.9	4.0	131	18
RNA methyltransferases											
VP39	1AV6	[39]	1.51	25	2.03	83	14	5.5	4.1	140	9
ErmAM	1YUB	[55]	2.15	38	2.15	85	12	4.2	4.4	142	11
ErmC	2ERC	[56]	0.94	31	2.06	108	15	7.7	3.6	140	11
fibrillarin	1FBN	[57]	0.98	19	1.66	109	21	9.7	3.1	150	18
Protein methyltransferases											
CheR	1AF7	[29]	0.64	19	1.66	103	17	7.8	2.6	122	15
Small molecule methyltransferases											
Glycine N-MTase	1D2H	[58]	0.70	31	1.65	111	16	7.9	2.8	130	17
Catechol O-MTase	1VID	[30]	0.47	50	1.39	72	22	9.3	2.8	144	14

[a] Alignment of the indicated structure against *T. maritima* PIMT obtained with the lsq_explicit and lsq_improve options in the program O [49].
[b] Alignment of the indicated structure against *T. maritima* PIMT obtained with the program DALI [31].
[c] Explicit initial alignment of the 16 residues of the β1 loop-αA region using the lsq_explicit option.
[d] Improved final alignment over the whole protein using the lsq_improve option.
[e] Root mean square deviation (rmsd) of 64 backbone atoms and sequence identity with *T. maritima* PIMT over the 16 aligned residues.
[f] Rmsd of Cα atoms and sequence identity with *T. maritima* PIMT over the indicated number of equivalent Cα atoms extracted from the final aligned structures with the program STRUPRO [51].
[g] Z score (in sigma units), rmsd of Cα atoms, and sequence identity with *T. maritima* PIMT over the indicated number of equivalent Cα atoms as determined by the program DALI [31].

isoaspartyl residues at those sites where they occur most often in proteins, perhaps assisted by coevolution of the most frequently damaged sites toward enhanced repairability by PIMT.

A Model PIMT-AdoMet-isoAsp Peptide Ternary Complex

We have conducted a modeling study to investigate the potential interactions of PIMT, AdoMet, and isoaspartyl peptide. The structure of COMT with AdoMet and the inhibitor 3,5-dinitrocatechol [30] was used as a model ternary complex. Our modeling assumed the absence of a conformational change in Ile-206, despite the positive charge on AdoMet, which would make the conformation of Ile-206 seen in the crystalline AdoHcy complex less favorable energetically. Since the conformation of Ile-206 seen in the crystalline AdoHcy complex is well-stabilized by nonpolar interactions with the phenyl ring of Tyr-55 and the C and Cα atoms of Ser-56, we propose that this conformation is retained in the ternary complex we have modeled.

The model suggests that the α-carboxylate oxygen of the isoaspartyl side chain could enter the deep well near the AdoHcy Sδ and approach within 2.6 Å of the modeled AdoMet Cϵ methyl group without significant steric clashes (Figure 5D). In the model complex, Ser-59 could form a strong hydrogen bond to the nonesterified α-carboxylate oxygen atom of the isoaspartate. Largely due to the positively charged AdoMet, the well has positive electrostatic potential that will interact favorably with the α-carboxylate (Figures 5b–5c). Removing the unique C-terminal domain of *T. maritima* PIMT slightly enhances the calculated positive potential around the well. This electrostatic interaction may explain the approximately 6-fold increase in affinity for isoAsp peptide when PIMT is bound to AdoMet versus AdoHcy [44].

It is difficult to determine from our modeling study exactly where the binding site for the residues on either side of isoAsp lies on the surface of the protein. While part of the isoAsp peptide most likely lies within the cleft between the two rims and another part may lie over the Ile-206 bridge, there is uncertainty even in the direction of the peptide backbone.

No matter the orientation, there would be multiple opportunities for the side chains of Tyr-55 and Thr-57 to interact with the peptide backbone near the isoAsp side chain. Immediately below the substrate well (in the orientation of Figures 2 and 5b–5c), on the far side of a constriction made by the side chain of Val-45 and the carbonyl of Arg-204, lies a groove composed of the side chains of Val-45, Gln-60, Leu-63, Met-64, Leu-201, Thr-203, and Phe-205. Despite being on the surface of the protein, many of these hydrophobic residues are highly conserved as part of PIMT sequence motifs II, III, and XII. This groove may provide a neutral, largely hydrophobic surface for binding part of the peptide substrate, perhaps the two residues preceding the isoAsp, where PIMT favors large, neutral side chains [42].

Catalytic Mechanism and Potential Conformational Changes

While we suggest that conformational changes are not required to bind an isoaspartyl peptide to a complex that already contains AdoMet, conformational changes may be needed at other steps in the catalytic cycle. Due to the nearly complete burial of AdoHcy, a substantial conformational change may be required to release it following methyl group transfer.

While kinetic studies have proposed various mechanisms for PIMT, the most careful recent study suggests that the mechanism is sequential and either random or ordered with AdoMet binding first [44]. The present crystal structure, with AdoHcy deeply buried beneath the proposed peptide recognition site, strongly supports the ordered mechanism with AdoMet binding first.

How does AdoHcy leave the active site (and AdoMet enter) to begin the next cycle? Perhaps the side chain of Ile-206 and residues of βb or the entire βa/βb hairpin move to allow the cofactors in and out. The B factors for residues of the βa/βb turn are among the highest in the structure.

Prospects

How isoaspartyl residues in a variety of proteins can be methylated given the extensive and specific surface that PIMT presents remains a crucial question to be answered in future studies. The well-ordered structure around the active site seems to greatly limit the range of isoaspartyl peptide conformations that could interact with the enzyme.

Proteases that recognize specific sequences in many three-dimensional contexts may be good structural models for PIMT recognition. Proteases interact with their target sequences in a single conformation. The various substrates must adopt that conformation for cleavage to occur, and the ability of the substrate to adopt the reactive conformation is an important determinant of its susceptibility to proteolysis. On the other hand, PIMT may also exhibit some plasticity in binding isoAsp peptides. The goal of our ongoing studies is to determine the conformation(s) that isoaspartyl substrates must adopt for PIMT recognition. Within these conformations lies the basis for understanding the relative effectiveness of PIMT in protecting cellular proteins from the chemical instability inherent in evolution's original "choice" to employ asparagine and aspartate as amino acids.

Biological Implications

Rearrangement of a protein backbone to form isoaspartate is a frequent occurrence at aspartate and asparagine residues. The backbone is lengthened by one methylene group at the isoaspartyl residue, and this damage frequently results in a loss of functional activity. To protect themselves from the damage that occurs as the result of isoaspartyl formation, nearly all organisms have a repair pathway catalyzed by the enzyme protein L-isoaspartate (D-aspartate) O-methyltransferase (PIMT). PIMT transfers a methyl group from S-adenosyl-L-methionine to the side chain of the isomerized aspartyl residue. Methyl transfer initiates a repair reaction that converts isoaspartate residues to normal aspartate ones. PIMT is a conserved enzyme, essential for life past 6 weeks in mice and for enhancing stationary phase survival in *E. coli*.

We have determined the first structure of a PIMT, using the stable and highly active enzyme from *T. maritima*. The protein forms a continuous structure but can be divided into three subdomains based on sequence, structure, and function. The N-terminal subdomain contains sequences homologous only to other PIMTs. The central subdomain resembles domains common to many other methyltransferases but with a rearrangement of β strands that is so far unique to PIMT.

Access to the methyl group donor site is restricted to a deep well between two ridges, which forms the putative isoaspartyl substrate binding site. The effectiveness of PIMT in repairing damaged proteins is dependent on its ability to recognize isoaspartyl residues in a wide variety of sequence and struc-

tural contexts and to discriminate against a large number of aspartyl and other carboxylate groups. While the structural basis of these phenomena in PIMT requires further study, the structure of *T. maritima* PIMT presents a rigid-appearing surface with an arrangement of hydrogen bonding and hydrophobic groups upon which recognition and discrimination must occur.

Experimental Procedures

Expression and Purification

The gene for *T. maritima* PIMT [26] was cloned from genomic DNA (TIGR) into the T7 expression vector pET30. Expressed protein was solubilized in 6 M urea, partially purified, and refolded by dialysis into solutions of 10 mM Tris-HCl (pH 8.6), 1 mM DTT, 5 mM β-mercaptoethanol, and 0.1 mM EDTA with decreasing concentrations of urea. Refolded PIMT in the same buffer without urea was purified on Q Sepharose Fast Flow and SOURCE 15Q (Pharmacia). Fractions containing PIMT were pooled, dialyzed into 10 mM Tris-HCl (pH 8.0), 1 mM DTT, 5 mM β-mercaptoethanol, 5% (v/v) glycerol, and 0.84 M ammonium sulfate and further purified on SOURCE 15ETH. PIMT was dialyzed into a final buffer consisting of 10 mM Tris-HCl (pH 8.0), 200 mM NaCl, 5% (v/v) glycerol, 1 mM DTT, 5 mM β-mercaptoethanol, 0.1 mM EDTA, and 0.02% (w/v) sodium azide, and concentrated to ~6 mg ml^{-1}.

Crystallization

Crystals were grown by hanging drop vapor diffusion at 18°C. Complexes with AdoHcy were formed by adding a 2-fold molar ratio of AdoHcy to the concentrated protein stock. Drops were formed by mixing 3 μl of the protein-AdoHcy complex with 3 μl of a reservoir solution containing 28% (v/v) PEG 400, 100 mM NaOAc (pH 4.5), and 100 mM $CdCl_2$ (or $ZnSO_4$). The enzyme crystallized in space group $P2_1$, with two monomers in the asymmetric unit. Unit cell dimensions were a = 51.06 Å, b = 98.91 Å, c = 76.86 Å, β = 105.66°. Crystals were transferred to a stabilization solution consisting of 40% PEG 400, 100mM NaOAc (pH 4.5), and 50mM $CdCl_2$ (or $ZnSO_4$) prior to flash freezing in a gaseous nitrogen stream at 100° K. Heavy atom derivatives were formed by soaking crystals in the same solution containing the heavy atom reagent before freezing.

Structure Determination

X-ray diffraction data were collected using an RAXIS IV on a rotating anode generator and reduced and scaled with the HKL suite [45]. The positions of two native cadmium sites and four lead sites in the trimethyllead acetate soak were readily determined by Patterson methods. Phases calculated from the Cd-native and first trimethyllead derivative were used to identify heavy atom sites in the remaining derivatives. Heavy atom sites were refined and initial phases calculated using MLPHARE [46]. Experimental phases were improved by density modification in the program DM [47], followed by the multiple automated refinement procedure of ARP/wARP [48].

The atomic model was built using the graphics program O [49]. The electron density map was unambiguous, and the two chains could be traced readily. Refinement was carried out using CNS [50] for five cycles of simulated annealing torsional dynamics followed by restrained individual B factor refinement and manual rebuilding in each cycle. Only the C-terminal residue of one monomer is absent from the final model. Several surface side chains in each subunit are disordered.

Structural Alignments

Alignment of 12 AdoMet-MTases of known structure to PIMT was conducted by two methods. In the first, the backbone atoms of 16 residues in the highly conserved β1 loop-αA region of the AdoMet-MTase fold were used to obtain an initial alignment with the lsq_explicit option of the program O [49]. The initial alignment was then improved using the lsq_improve option, employing the default settings. The second method was pairwise superposition of each AdoMet-MTase onto PIMT with the program DALI [31].

The program STRUPRO [51] extracted equivalent sequences from the lsq_improve aligned structures to generate a structure-based sequence alignment (Figure 3b). The default settings were employed with the exception that fragments as short as 3 residues were considered for alignment. Due to the difficulty of depicting a multiple sequence alignment for all the AdoMet-MTases in limited space, only a portion of the multiple-sequence alignment is shown.

Modeling of Ternary Complex with AdoMet and Isoaspartyl Peptide

The structure of COMT containing AdoMet and the inhibitor 3,5-dinitrocatechol [30] (PDB entry 1vid) was used as the basis for modeling a ternary complex of PIMT with AdoMet and isoaspartyl peptide. Superposition of the Cα coordinates of COMT onto PIMT (Table 3) was the starting point for the modeling. The location of COMT's AdoMet relative to AdoHcy in the binding site of PIMT was further adjusted by superimposing the ribose and homocysteine atoms of AdoMet onto AdoHcy. The superimposed AdoMet coordinates were used for the ternary complex model, and the same superposition operator was used to make a small adjustment to the position of the inhibitor.

Isoaspartyl 67 RNase A [17] (PDB entry 1dy5) was employed as the source of a peptide fragment for modeling. A fragment containing the isoaspartyl residue was extracted from the structure, and the α-carboxylate oxygens of the isoaspartyl residue were manually aligned with the vicinal hydroxyls of 3,5-dinitrocatechol, avoiding steric clashes with PIMT.

Electrostatic Potential Calculations

Electrostatic surface potential was calculated in the program GRASP [52] using the standard partial charges, the default dielectric constants, and 0 mM salt concentration. AdoMet was assigned partial charges based on those for similar groups in the topology files of CNS [50].

Acknowledgments

A. M. F. would like to thank Dr. Peter Blier for first bringing isoaspartyl formation to his attention. We would like to thank Dr. V. Jo Davisson for helpful discussions and Dr. Karen Nelson and the Institute for Genomics Research for the gift of *T. maritima* genomic DNA. Earlier studies on mammalian PIMT were supported by a pilot study grant from the National Institute on Aging (RO3 AG14838).

Received: June 28, 2000
Revised: September 4, 2000
Accepted: September 22, 2000

References

1. Visick, J.E., and Clarke, S. (1995). Repair, refold, recycle: how bacteria can deal with spontaneous and environmental damage to proteins. Mol. Microbiol. *16*, 835–845.
2. Battersby, A.R., and Robinson, J.C. (1955). Studies on specific chemical fission of peptide links. Part I. The rearrangement of aspartyl and glutamyl peptides. J. Chem. Soc. *1955*, 259–269.
3. Geiger, T., and Clarke, S. (1987). Deamidation, isomerization, and racemization at asparaginyl and aspartyl residues in peptides. Succinimide-linked reactions that contribute to protein degradation. J. Biol. Chem. *262*, 785–794.
4. Voorter, C.E., de Haard-Hoekman, W.A., van den Oetelaar, P.J., Bloemendal, H., and de Jong, W.W. (1988). Spontaneous peptide bond cleavage in aging alpha-crystallin through a succinimide intermediate. J. Biol. Chem. *263*, 19020–19023.
5. Teshima, G., Stults, J.T., Ling, V., and Canova-Davis, E. (1991). Isolation and characterization of a succinimide variant of methionyl human growth hormone. J. Biol. Chem. *266*, 13544–13547.
6. Bischoff, R., et al., and Roitsch, C. (1993). Sequence-specific deamidation: isolation and biochemical characterization of succinimide intermediates of recombinant hirudin. Biochemistry *32*, 725–734.
7. Tomizawa, H., Yamada, H., Ueda, T., and Imoto, T. (1994). Isolation and characterization of 101-succinimide lysozyme that possesses the cyclic imide at Asp101-Gly102. Biochemistry *33*, 8770–8774.
8. Noguchi, S., Miyawaki, K., and Satow, Y. (1998). Succinimide and isoaspartate residues in the crystal structures of hen egg-white lysozyme complexed with tri-N-acetylchitotriose. J. Mol. Biol. *278*, 231–238.
9. Stephenson, R.C., and Clarke, S. (1989). Succinimide formation from aspartyl and asparaginyl peptides as a model for the spontaneous degradation of proteins. J. Biol. Chem. *264*, 6164–6170.
10. Johnson, B.A., Shirokawa, J.M., Hancock, W.S., Spellman, M.W., Basa, L.J., and Aswad, D.W. (1989). Formation of isoaspartate at two distinct sites during *in vitro* aging of human growth hormone. J. Biol. Chem. *264*, 14262–14271.
11. Johnson, B.A., Murray, E.D., Jr., Clarke, S., Glass, D.B., and Aswad, D.W. (1987). Protein carboxyl methyltransferase facilitates conversion

of atypical L-isoaspartyl peptides to normal L-aspartyl peptides. J. Biol. Chem. *262*, 5622–5629.
12. McFadden, P.N., and Clarke, S. (1987). Conversion of isoaspartyl peptides to normal peptides: implications for the cellular repair of damaged proteins. Proc. Natl. Acad. Sci. USA *84*, 2595–2599.
13. Di Donato, A., Ciardiello, M.A., de Nigris, M., Piccoli, R., Mazzarella, L., and D'Alessio, G. (1993). Selective deamidation of ribonuclease A. Isolation and characterization of the resulting isoaspartyl and aspartyl derivatives. J. Biol. Chem. *268*, 4745–4751.
14. Yamada, H., et al., and Imoto, T. (1985). Isolation and characterization of 101-beta-lysozyme that possesses the beta-aspartyl sequence at aspartic acid-101. Biochemistry *24*, 7953–7959.
15. Wearne, S.J., and Creighton, T.E. (1989). Effect of protein conformation on rate of deamidation: ribonuclease A. Proteins *5*, 8–12.
16. Chazin, W.J., Kordel, J., Thulin, E., Hofmann, T., Drakenberg, T., and Forsen, S. (1989). Identification of an isoaspartyl linkage formed upon deamidation of bovine calbindin D9k and structural characterization by 2D 1H NMR. Biochemistry *28*, 8646–8653.
17. Capasso, S., et al., and Mazzarella, L. (1996). Deamidation in proteins: the crystal structure of bovine pancreatic ribonuclease with an isoaspartyl residue at position 67. J. Mol. Biol. *257*, 492–496.
18. Noguchi, S., Satow, Y., Uchida, T., Sasaki, C., and Matsuzaki, T. (1995). Crystal structure of *Ustilago sphaerogena* ribonuclease U2 at 1.8 Å resolution. Biochemistry *34*, 15583–15591.
19. Johnson, B.A., Langmack, E.L., and Aswad, D.W. (1987). Partial repair of deamidation-damaged calmodulin by protein carboxyl methyltransferase. J. Biol. Chem. *262*, 12283–12287.
20. Brennan, T.V., Anderson, J.W., Jia, Z., Waygood, E.B., and Clarke, S. (1994). Repair of spontaneously deamidated HPr phosphocarrier protein catalyzed by the L-isoaspartate-(D-aspartate) O-methyltransferase. J. Biol. Chem. *269*, 24586–24595.
21. Johnson, B.A., Ngo, S.Q., and Aswad, D.W. (1991). Widespread phylogenetic distribution of a protein methyltransferase that modifies L-isoaspartyl residues. Biochem. Int. *24*, 841–847.
22. O'Connor, C.M., and Clarke, S. (1985). Specific recognition of altered polypeptides by widely distributed methyltransferases. Biochem. Biophys. Res. Commun. *132*, 1144–1150.
23. Li, C., and Clarke, S. (1992). Distribution of an L-isoaspartyl protein methyltransferase in eubacteria. J. Bacteriol. *174*, 355–361.
24. Kim, E., Lowenson, J.D., MacLaren, D.C., Clarke, S., and Young, S.G. (1997). Deficiency of a protein-repair enzyme results in the accumulation of altered proteins, retardation of growth, and fatal seizures in mice. Proc. Natl. Acad. Sci. USA *94*, 6132–6137.
25. Visick, J.E., Cai, H., and Clarke, S. (1998). The L-isoaspartyl protein repair methyltransferase enhances survival of aging *Escherichia coli* subjected to secondary environmental stresses. J. Bacteriol. *180*, 2623–2629.
26. Ichikawa, J.K., and Clarke, S. (1998). A highly active protein repair enzyme from an extreme thermophile: the L-isoaspartyl methyltransferase from *Thermotoga maritima.* Arch. Biochem. Biophys. *358*, 222–231.
27. Laskowski, R.A., MacArthur, M.W., Moss, D.W., and Thornton, J.M. (1993). PROCHECK - a program to check the stereochemical quality of proteins. J. Appl. Crystallogr. *26*, 283–291.
28. Schluckebier, G., O'Gara, M., Saenger, W., and Cheng, X. (1995). Universal catalytic domain structure of AdoMet-dependent methyltransferases. J. Mol. Biol. *247*, 16–20.
29. Djordjevic, S., and Stock, A.M. (1997). Crystal structure of the chemotaxis receptor methyltransferase CheR suggests a conserved structural motif for binding S-adenosylmethionine. Structure *5*, 545–558.
30. Vidgren, J., Svensson, L.A., and Liljas, A. (1994). Crystal structure of catechol O-methyltransferase. Nature *368*, 354–358.
31. Holm, L., and Sander, C. (1993). Protein structure comparison by alignment of distance matrices. J. Mol. Biol. *233*, 123–138.
32. Thompson, J.D., Higgins, D.G., and Gibson, T.J. (1994). CLUSTAL W: improving the sensitivity of progressive multiple sequence alignment through sequence weighting, position-specific gap penalties and weight matrix choice. Nucleic Acids Res. *22*, 4673–4680.
33. Kagan, R.M., and Clarke, S. (1994). Widespread occurrence of three sequence motifs in diverse S-adenosylmethionine-dependent methyltransferases suggests a common structure for these enzymes. Arch. Biochem. Biophys. *310*, 417–427.
34. Zhang, X., Zhou, L., and Cheng, X. (2000). Crystal structure of the conserved core of protein arginine methyltransferase PRMT3. EMBO J. *19*, 3509–3519.
35. Bugl, H., et al., and Jakob, U. (2000). RNA methylation under heat shock control. Mol. Cell *6*, 349–360.
36. Sheikhnejad, G., et al., and Cheng, X. (1999). Mechanism of inhibition of DNA (cytosine C5)-methyltransferases by oligodeoxyribonucleotides containing 5,6-dihydro-5-azacytosine. J. Mol. Biol. *285*, 2021–2034.
37. Reinisch, K.M., Chen, L., Verdine, G.L., and Lipscomb, W.N. (1995). The crystal structure of HaeIII methyltransferase convalently complexed to DNA: an extrahelical cytosine and rearranged base pairing. Cell *82*, 143–153.
38. Labahn, J., et al., and Saenger, W. (1994). Three-dimensional structure of the adenine-specific DNA methyltransferase M.Taq I in complex with the cofactor S-adenosylmethionine. Proc. Natl. Acad. Sci. USA *91*, 10957–10961.
39. Hodel, A.E., Gershon, P.D., and Quiocho, F.A. (1998). Structural basis for sequence-nonspecific recognition of 5′-capped mRNA by a cap-modifying enzyme. Mol. Cell *1*, 443–447.
40. Kabsch, W., and Sander, C. (1983). Dictionary of protein secondary structure: pattern recognition of hydrogen-bonded and geometrical features. Biopolymers *22*, 2577–2637.
41. O'Connor, C.M., and Clarke, S. (1985). Analysis of erythrocyte protein methyl esters by two-dimensional gel electrophoresis under acidic separating conditions. Anal. Biochem. *148*, 79–86.
42. Lowenson, J.D., and Clarke, S. (1991). Structural elements affecting the recognition of L-isoaspartyl residues by the L-isoaspartyl/D-aspartyl protein methyltransferase. Implications for the repair hypothesis. J. Biol. Chem. *266*, 19396–19406.
43. Jamaluddin, M., Kim, S., and Paik, W.K. (1976). A comparison of kinetic parameters of polypeptide substrates for protein methylase II. Biochemistry *15*, 3077–3081.
44. Johnson, B.A., and Aswad, D.W. (1993). Kinetic properties of bovine brain protein L-isoaspartyl methyltransferase determined using a synthetic isoaspartyl peptide substrate. Neurochem. Res. *18*, 87–94.
45. Otwinowski, Z., and Minor, W. (1997). Processing of x-ray diffraction data collected in oscillation mode. Methods Enzymol. *276*, 307–326.
46. Otwinowski, Z. (1991). Isomorphous refinement and anomalous scattering. In Proceedings of the CCP4 Study Weekend, W. Wolf et al., eds. (Daresbury, UK: SERC Daresbury Lab), pp. 80–86.
47. Cowtan, K. (1994). "DM": an automated procedure for phase improvement by density modification. Joint CCP4 ESF-EACBM Newsletter Protein Crystallogr. *31*, 34–38.
48. Perrakis, A., Morris, R., and Lamzin, V.S. (1999). Automated protein model building combined with iterative structure refinement. Nat. Struct. Biol. *6*, 458–463.
49. Jones, T.A., and Kjeldgaard, M. (1997). Electron-density map interpretation. Methods Enzymol. *276*, 173–207.
50. Brunger, A.T., et al., and Warren, G.L. (1998). Crystallography & NMR system: a new software suite for macromolecular structure determination. Acta Crystallogr. D *54*, 905–921.
51. Kleywegt, G.J., and Jones, T.A. (1998). Databases in protein crystallography. Acta Crystallogr. D *54*, 1119–1131.
52. Nicholls, A., Bharadwaj, R., and Honig, B. (1993). GRASP: graphical representation and analysis of surface properties. Biophys. J. *64*, A166.
53. Tran, P.H., Korszun, Z.R., Cerritelli, S., Springhorn, S.S., and Lacks, S.A. (1998). Crystal structure of the DpnM DNA adenine methyltransferase from the DpnII restriction system of *Streptococcus pneumoniae* bound to S-adenosylmethionine. Structure *6*, 1563–1575.
54. Gong, W., O'Gara, M., Blumenthal, R.M., and Cheng, X. (1997). Structure of Pvu II DNA-(cytosine N4) methyltransferase, an example of domain permutation and protein fold assignment. Nucleic Acids Res. *25*, 2702–2715.
55. Yu, L., et al., and Fesik, S.W. (1997). Solution structure of an rRNA methyltransferase (ErmAM) that confers macrolide-lincosamide-streptogramin antibiotic resistance. Nat. Struct. Biol. *4*, 483–489.
56. Bussiere, D.E., et al., and Abad-Zapatero, C. (1998). Crystal structure of ErmC', an rRNA methyltransferase which mediates antibiotic resistance in bacteria. Biochemistry *37*, 7103–7112.
57. Wang, H., Boisvert, D., Kim, K.K., Kim, R., and Kim, S.H. (2000). Crystal structure of a fibrillarin homologue from Methanococcus jannaschii, a hyperthermophile, at 1.6 Å resolution. EMBO J. *19*, 317–323.
58. Huang, Y., et al., and Takusagawa, F. (2000). Mechanisms for autoinhibition and forced product release in glycine N-methyltransferase: crystal structures of wild-type, mutant R175K and S-adenosylhomocysteine-bound R175K enzymes. J. Mol. Biol. *298*, 149–162.
59. Kraulis, P.J. (1991). MOLSCRIPT: a program to produce both detailed

and schematic plots of protein structures. J. Appl. Crystallogr. *24*, 946–950.
60. Schluckebier, G., Kozak, M., Bleimling, N., Weinhold, E., and Saenger, W. (1997). Differential binding of S-adenosylmethionine, S-adenosylhomocysteine and Sinefungin to the adenine-specific DNA methyltransferase M.TaqI. J. Mol. Biol. *265*, 56–67.
61. Sander, C., and Schneider, R. (1991). Database of homology-derived protein structures and the structural meaning of sequence alignment. Proteins *9*, 56–68.
62. Barton, G.J. (1993). ALSCRIPT: a tool to format multiple sequence alignments. Protein Eng. *6*, 37–40.

Accession Numbers

Coordinates and structure factors for *T. maritima* PIMT complexed to AdoHcy have been deposited at the PDB, accession code 1dl5.